Surface Science 291 (1993) 395–401
North-Holland

surface science

Termination layer variations on the cleaved $Rb_{1/3}WO_3(0001)$ surface determined by scanning tunneling microscopy

Weier Lu [a], Neysa Nevins [b], Michael L. Norton [c] and Gregory S. Rohrer [a]

[a] *Department of Materials Science and Engineering, Carnegie Mellon University, Pittsburgh, PA 15213, USA*
[b] *Department of Chemistry, University of Georgia, Athens, GA 30602, USA*
[c] *Department of Chemistry, Marshall University, Huntington, WV 25701, USA*

Received 22 February 1993; accepted for publication 25 March 1993

Cleaved (0001) surfaces of the hexagonal tungsten bronze, $Rb_{1/3}WO_3$, were studied by scanning tunneling microscopy (STM). Cleavage produces flat terraces with micron-scale dimensions that are separated by straight surface steps with heights equal to one half or one unit cell. High resolution images show that the well-ordered surface layers are occasionally interrupted by point defects. Two different contrast patterns with the periodicity of the bulk structure were observed and assigned to two different termination layers. The presence of different termination layers is an expected consequence of the cleavage process. Comparing the constant current STM images with ideal structures indicates that in this case image contrast is dominated by differences in the relative vertical positions of the surface atoms.

1. Introduction

Efforts to determine the structure of transition metal oxide surfaces have been motivated by the premise that the atomic-level structure is linked to technologically important surface related processes such as chemical reactivity. In recent years, scanning tunneling microscopy (STM) has had an impact on oxide surface structure determinations; several three-dimensionally bonded oxides [1–3] and several layered oxides [4–6] have already been imaged at atomic-scale resolution. We have used this technique to study the surface structure of the hexagonal tungsten bronze (HTB) $Rb_{1/3}WO_3$. This compound is one member of the larger family of alkali tungsten bronzes; materials that have been subjected to numerous surface studies in the past because their stoichiometric versatility offers an opportunity to probe the manner in which the structure, composition, and properties of the surface are affected by those of the bulk [7–10].

One distinct advantage of STM is that it is a local probe capable of imaging non-periodic structural components. The features of primary interest in this paper are the inhomogeneities in the surface termination layer. Variations in the surface termination layer have received little attention, yet are the inevitable result when the surfaces of most three-dimensionally bonded compounds are created at low homologous temperatures by mechanical processes such as cleavage, fracture, and wear. We present here images of two different termination layers found on cleaved HTB surfaces.

The HTB structure of $Rb_{1/3}WO_3$ was originally determined by Magnéli [11] and has more recently been refined by Labbé et al. [12]. The exact composition of this compound varies with preparation and has been reported in the range $Rb_{0.27}WO_3$ to $Rb_{0.30}WO_3$; for simplicity we will refer to it using the ideal formula $Rb_{1/3}WO_3$. The structure is most easily visualized as a network of corner sharing WO_6 octahedral units, as shown in fig. 1. In planes parallel to (0001), the octahedra link in a hexagonal pattern which leaves cavities in the structure. The layers are then stacked so that the cavities form tunnels parallel

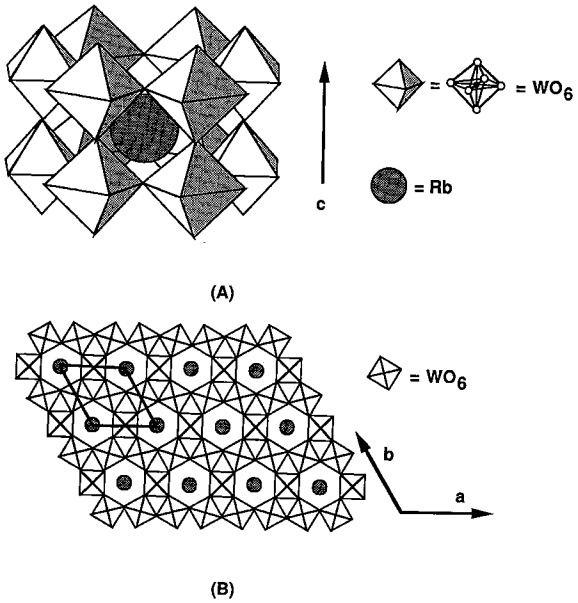

Fig. 1. Idealized polyhedral representation of the HTB structure. Each corner of the octahedral unit is shared between two octahedra, as shown in (a). The projection down the c-axis (b) shows the hexagonal arrangement in layers normal to c. The layers stack to form tunnels along c which house the Rb cations.

to the c-axis. The Rb ions occupy sites within the tunnels and are coordinated by 12 O ions. The three-dimensional unit cell is hexagonal with dimensions $a = 7.3875(11)$ Å and $c = 7.5589(12)$ Å [12] and the planar unit of the unreconstructed (0001) surface is also hexagonal with $a = b = 7.39$ Å. For the discussion in this paper it is important to recognize the unique six-fold axis of rotational symmetry that runs parallel to the c-axis, through the Rb ions sites in the tunnel.

2. Experimental procedure

Single crystals of $Rb_{1/3}WO_3$ were grown using a seeded chemical vapor recrystallization technique [13]. All materials were used as purchased. Rb_2WO_4 was obtained 99.9% pure from Cerac, Inc., WO_3 from Alfa Products (99.7%), W metal (99.5%) and $TeCl_4$ (99%) from ROC/RIC. A ten gram mixture of the oxides and tungsten metal was prepared according to the formula:

$$x/2 \cdot Rb_2WO_4 + [1 - (2x/3)] \cdot WO_3 + x/6 \cdot W \rightarrow Rb_xWO_3,$$

where $x = 0.33$. To eliminate moisture from these high surface area powders, the mixture was heated to 230°C in dynamic vacuum for 24 h in an 18 cm long fused quartz ampule made from 15 × 20 mm tubing from Quartz Scientific. Before introduction of 20 mg of the volatile crystallizing agent $TeCl_4$, the ampule was cooled to room temperature under vacuum, the transport agent was quickly introduced, the ampule was pumped down and sealed when a pressure of 7 μm was attained. The materials were slowly ramped to 1060°C over a 24 h period, and remained at 1060°C for 96 h. The ampule was slowly cooled to room temperature over a 24 h period to prevent thermal shock to the ampule, which was attacked by alkali, as is commonly observed in bronze growths. Although some crystals formed by transport due to adventitious temperature gradients in the three zone tube furnace employed, the crystals used in this study grew by recrystallization of the powdered material. Reaction and growth with the crystallization aid ($TeCl_4$) leads to crystals with maximum dimensions 10 to 20 times greater than growths performed without this agent. Preliminary studies using I_2 have not found it to be a useful aid in growing this phase.

The dark blue metallic crystals displayed the expected hexagonal prismatic morphology and were characterized using energy-dispersive analysis of X-rays (EDX) and powder X-ray diffraction (XRD). EDX analysis of cleaved crystals confirms the presence of Rb and W as major components. Within the detection limit of EDX (about 2 at%), the interior of the crystals was not contaminated by Te or Cl. Several representative crystals were pulverized for the XRD analysis. The powder pattern unambiguously identified the phase as $Rb_{1/3}WO_3$. The lattice parameters, determined from a least squares refinement of 30 well-measured reflections, were $a = 7.3945(8)$ and $c = 7.5661(16)$. These parameters are in close agreement with those reported by Labbé et al. [12].

The observation of a 0.3% expansion of the cell volume suggests a slight difference in the Rb content.

The well-developed prismatic and basal facets (1–2 mm) were used as a basis for orientation. Fresh (0001) surfaces were made by cleavage in air immediately before insertion into the vacuum chamber which had a base pressure of less than 1×10^{-9} Torr. The tips used in these experiments were formed by clipping Pt–10%Ir wire. All of the images were acquired in the constant current mode using a 0.3 to 0.5 V sample bias (tunneling to unoccupied sample states) and a tunnel current of 0.6 to 0.8 nA. Attempts to image at small negative biases (tunneling from occupied sample states just below the Fermi level) failed. Furthermore, the position of the Fermi level in the conduction band and the ~ 3 eV gap between the valence and conduction bands makes the possibility of forming images from occupied valence band states unlikely. The average tunnel barrier, determined from measurements of the variation of current with vertical tip displacement, was 1.6 eV. Images presented here are representative of many observations of several specimens, more than 50 of which were recorded. The reproducibility of these observations leads us to believe that the different images reflect differences in the surface structures, rather than tip shape related artifacts. The images are presented in a gray scale in which the white-to-black contrast represents the top-to-bottom vertical height variation. The contrast scales on each image are adjusted to optimize the visual effect and a digital filter was used to remove high frequency noise.

3. Results and discussion

Typical cleaves produced surfaces that had vertical variations of less than 10 Å over areas as large as one square micron. Fig. 2 shows an image of the HTB(0001) surface which features several terraces separated by single (1/2c) or double (c) layer steps oriented along the high symmetry [11$\bar{2}$0] direction. We note that although this material has strong W–O bonds in all three dimensions, the perfection of the cleaves is characteristic of a layered material with highly anisotropic bonding. However, we also note that the resistance of this material to surface modification is more characteristic of a three-dimensional material. For the HTB, surface alterations were possible only when the tunneling bias was lowered far enough (< 0.02 V) to bring the tip in contact with the sample. In some layered materials, surface modification occurs under normal scanning conditions [14].

Fig. 2. 2150 Å × 2150 Å constant current image of the cleaved HTB surface. Changes in contrast correspond to steps oriented in the [11$\bar{2}$0] direction. The vertical height (black-to-white) is 10 Å.

Fig. 3 shows a higher resolution image where two-dimensional periodicity is apparent. The bright, irregular features were present on all areas of the samples and are either point defects or, more likely, surface adsorbates created during the time that the sample is exposed to air. The cleanliness of the surface, even after exposure to air, suggests either that these surfaces are relatively inert, or that scanning in vacuum somehow cleans the surface.

Higher resolution images show the detailed structure of the unit cell. We have observed two complementary types of images, shown in fig. 4. Both have the hexagonal symmetry of the bulk structure and even preserve the bulk unit cell

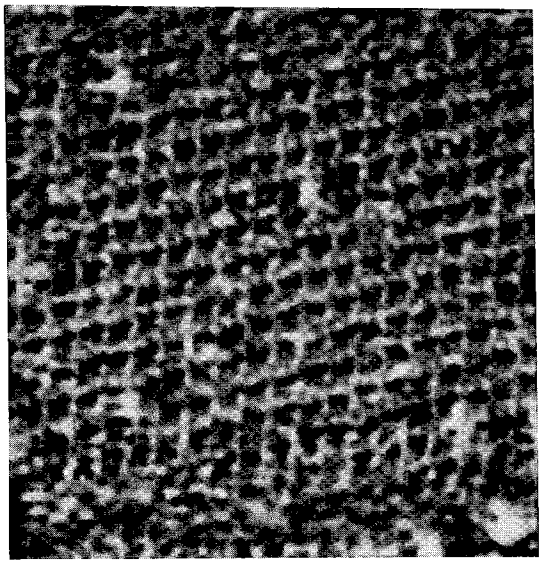

Fig. 3. 132 Å × 132 Å constant current image. The repeating pattern has the periodicity of the bulk unit cell. The protrusions (white spots) are the most common type of surface disorder. The vertical height (black-to-white) is 2 Å.

dimensions. However, the six-fold symmetry axes of these two images are at contrary positions: at depressions (black) in fig. 4a and at protrusions (white) in fig. 4b. Recall that a projection along the *c*-axis of the bulk structure has a unique center of six-fold rotational symmetry which is located at the center of the hexagonal channel where the Rb cations reside. Thus, the point of six-fold symmetry on the images must also represent this point. To understand the origin of these two types of contrast and the atomic structure of the surfaces, we consider the cleavage process at the atomic level.

To begin with, we ignore the Rb and consider only the W–O framework. Cleaving normal to [0001] breaks only the longitudinal W–O bond that connects the apical oxygen anion and the W cation (see fig. 5a). This creates two distinct complementary (0001) surfaces, one terminated by the W and the in-plane oxygen (labeled 2) and the other by the apical oxygen (labeled 3). Finally, we note that the Rb in this plane might go with either side, so that there are actually four distinct possibilities, as shown schematically in fig. 5a. Fig. 5b shows projected hard sphere models for each case, where the atoms are shaded according to their relative heights.

STM image contrast is determined primarily by a convolution of two factors: the surface elec-

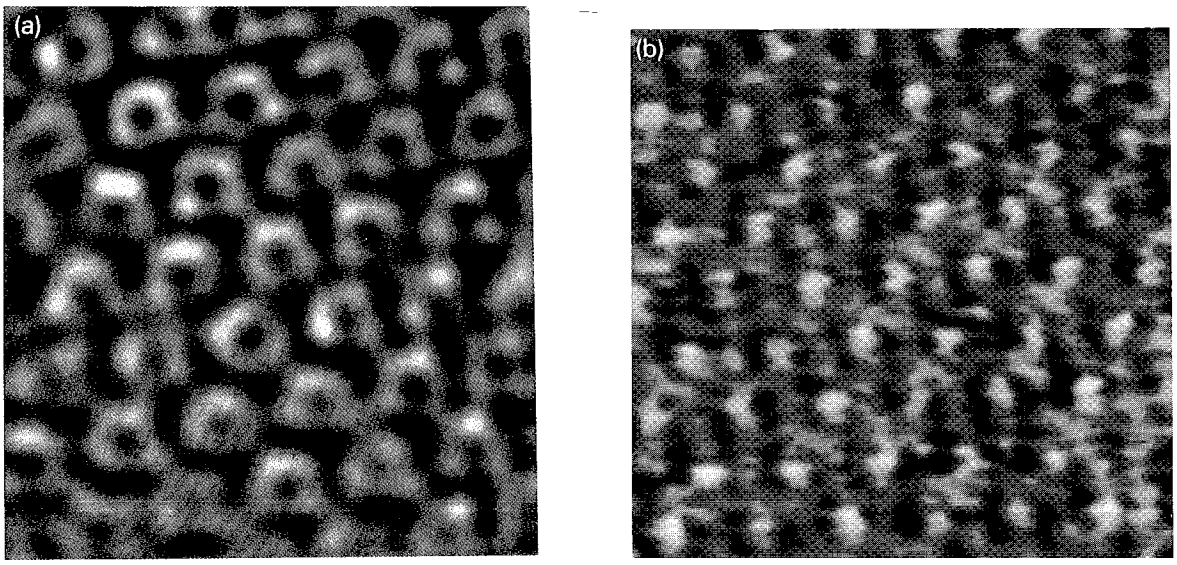

Fig. 4. (a) 44 Å × 44 Å constant current image, the vertical height (black-to-white) is 0.8 Å. There is a six-fold axis of rotational symmetry at the black point in the center of the rings. (b) 44 Å × 44 Å constant current image, the vertical height (black-to-white) is 2.0 Å. The elevated features (bright contrast) form a pattern with six-fold symmetry and the periodicity of the bulk unit cell.

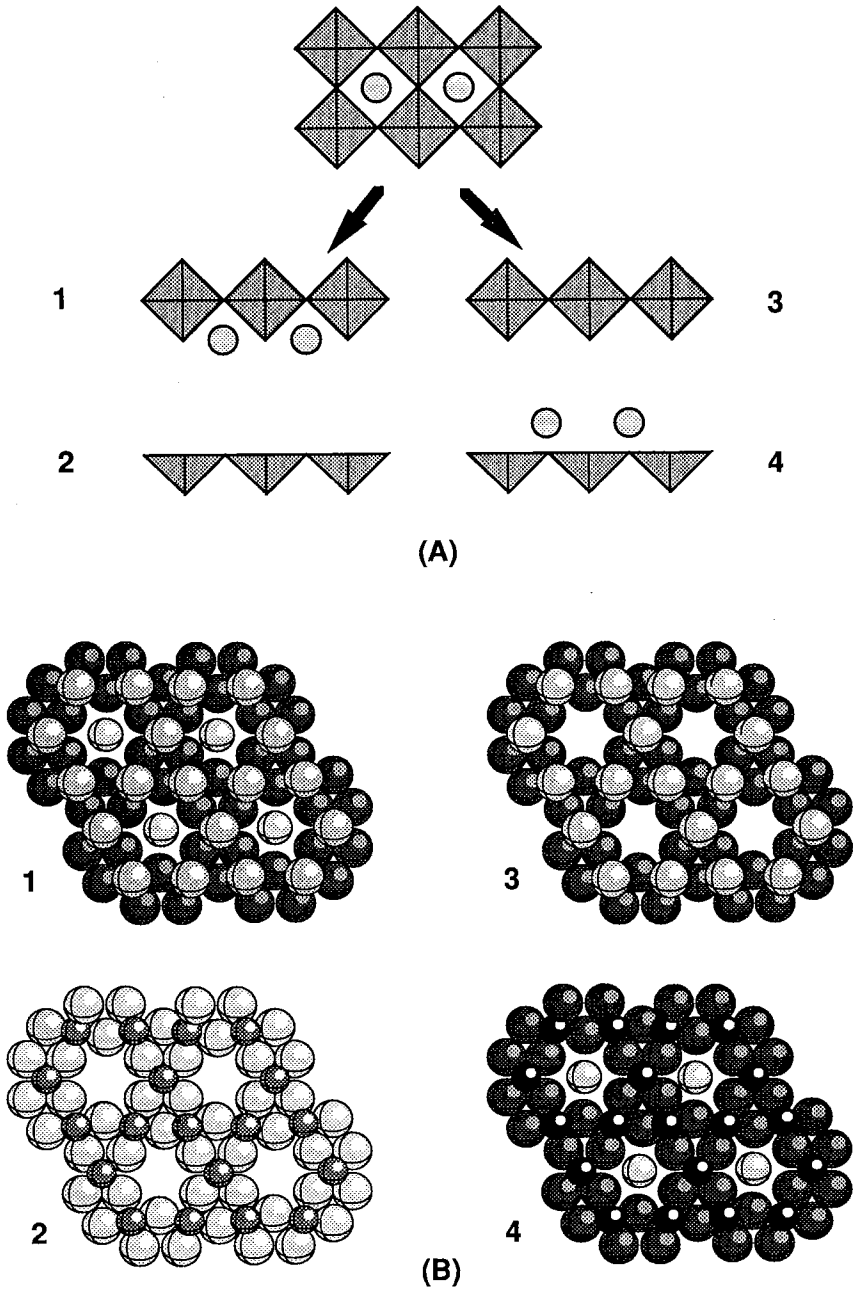

Fig. 5. (A) The cleavage of a corner-sharing octahedral network is shown schematically. For the case of the HTB, breaking bonds parallel to the *c*-axis must leave half of the W atoms in five-fold coordination and half in six-fold coordination. The Rb atoms can go to either side. (B) Hard sphere model of possible HTB surface structures projected along the *c*-axis. The Rb atoms appear inside the tunnels in 1 and 4, the W atoms are the smaller spheres in 2 and 4, and the O are the large spheres in all models. The spheres are shaded according to relative height above the surface plane, with lighter shades corresponding to greater elevations.

tronic structure and the relative vertical positions of the surface atoms. Attempts to deconvolute these two effects must be based on knowledge of the electronic structure. In this case, detailed information is unavailable, but we can refer to the chemically similar cubic tungsten bronze (CTB), Na_xWO_3, whose band structure has been described first in general terms by Goodenough [15] and later in more detail by Bullett [16]. While the electronic structures of these two materials are certainly not identical, we expect a qualitative similarity.

In the pure WO_3, the Fermi level lies midway between π and π^* bands formed by the overlap of O 2p and W 5d t_{2g} orbitals. However, because the π^* levels are always lower than the Rb 5s levels, electrons from the added alkali simply fill this initially empty band, raising the Fermi level with the alkali concentration. Because we formed our images by tunneling to states near the Fermi level, the contrast is determined by the orbitals that make up the π^* band. Bullett's [16] calculations indicate that the alkali does not contribute significantly to the bonding in the CTB, accounting for only 1% of the total conduction-band states, whereas O derived states contribute 20% and the balance is made up by W. Thus, all other factors being equal, we would expect the STM to be most sensitive to W, somewhat less sensitive to O and nearly insensitive to Rb.

The second important factor is the relative separation between the surface atoms and the tunneling tip. This factor, which we refer to as the proximity effect, is very important since the tunnel current is exponentially dependent on the sample–tip separation. For example, assuming that the W and O lie in the same plane and that the relative radial extent of their associated wave functions is given by their ionic radii, the O anion extends 0.75 Å further from the surface than the W cation. Again, if all other factors are equal, and we use the measured tunnel barrier height (1.6 eV), the tunnel current from the O atoms is 3.4 times greater than from W atoms in the same plane. Using the same reasoning, the Rb would make a dominant contribution to the tunnel current only if it extends 2.8 Å further from the surface than the W or O. Although the considerations here are clearly approximate, they provide a context within which the experimentally observed images can be compared to possible surface structures.

Considering first the image in fig. 4a, the depressions at the centers of six-fold symmetry indicate that this is the location of the Rb site and that this is an image of a surface where that Rb ion is not significantly elevated above the W and O and thus does not make a significant contribution to the tunnel current. The three possibilities are therefore surface 1 (O–Rb terminated), 2 (W–O terminated), or 3 (O terminated), shown in fig. 5b. We can differentiate between these choices by first noting that on surface 3 the apical O atoms should dominate the image contrast and form a hexagonal network of overlapping rings. Although the Rb ions on surface 1 are slightly higher than the apical O, it would not be enough to make a substantial contribution to the tunneling current and the same pattern of overlapping rings is expected for this surface. The isolated rings that are actually observed have the approximate positions of the in-plane O atoms on surface 2, assuming that the individual O atoms are not resolved. In this case, it appears that the proximity effect dominates the electronic structure effect, since the W atoms are not imaged.

Assuming that the topographic peaks in the image in fig. 4a correspond directly to the in-plane O positions in a unit cell with dimensions $a = b = 7.39$ Å, then the image suggests that the surface oxygen atoms have relaxed away from their bulk positions, 0.3 Å toward the center of the tunnel. While such a relaxation would suggest unusually short O–O separations, they would be nearly identical to the in-plane oxygen positions in the metastable hexagonal WO_3 which also has the HTB structure, but contains no alkali [17]. Thus, such a relaxation might be expected for the surface layer where at least half of the coordinating alkali atoms are missing. It is also possible that the peak in orbital density at this energy does not exactly correspond to the atomic position.

In fig. 4b, the protrusions at the centers of six-fold symmetry suggest that the Rb atoms are imaged. Based only on bonding considerations

discussed above, this seems unlikely. However, we note that the configuration of surface 4 (Rb terminated) situates the Rb atoms in positions that extend 2.3 Å further from the surface than the O atoms and 3 Å further than the W atoms. These relative positions, taken together with the approximate considerations discussed earlier in this section (that the barrier height is 1.6 eV, that Rb states make up 1% of the conduction band, O states 20% and W states the balance), leads to the conclusion that the Rb atom makes a dominate contribution to the tunneling current when the tip is over the Rb atom site. As in the case of the W–O terminated surface, it appears that the proximity effect dominates the contrast in the constant current images and in each case we preferentially image the atoms closest to the tip.

We have not observed any evidence of a domain structure in the termination layer. In our opinion, it is more likely that this is due to the small size of the areas that we are able to image with sufficient resolution, rather than to the absence of domains. We hope that further observations will clarify this point and lead to a statistical description of the composition of the termination layer.

4. Conclusion

By examining cleaved surfaces of $Rb_{0.33}WO_3$ with the STM, we have detected two different termination layers, W–O and Rb. For both cases we find that the surfaces are unreconstructed and that the proximity of the atoms in the surface layer dominates the image contrast. These surfaces are not necessarily the equilibrium surfaces, but rather characteristic of those produced by mechanical processes at low homologous temperatures. The ability of the STM to probe small areas of the surface makes it ideal for the study of the local structure of heterogeneous surfaces.

Acknowledgements

This work was supported at Carnegie Mellon University by the National Science Foundation under Grant DMR-9107305 and under Grant CHE-9215173 at Marshall University.

References

[1] G.S. Rohrer, V.E. Henrich and D.A. Bonnell, Science 250 (1990) 1239.
[2] R. Wiesendanger, I.V. Shvets, D. Bürgler, G. Tarrach, H.J. Güntherodt, J.M.D. Coey and S. Gräser, Science 255 (1992) 583.
[3] T. Matsumoto, H. Tanaka, T. Kawai and S. Kawai, Surf. Sci. Lett. 278 (1992) L153.
[4] J. Heil, J. Wesner, B. Lommel, W. Assmus and W. Grill, J. Appl. Phys. 65 (1989) 5220.
[5] Z. Zhang and C. Lieber, J. Phys. Chem. 96 (1992) 2030.
[6] G.S. Rohrer, W. Lu, R. Smith and A. Hutchinson, Surf. Sci., in press.
[7] M.A. Langell and S.L. Bernasek, J. Vac. Sci. Technol. 17 (1980) 1287.
[8] H. Hochst, R.D. Brigans and H.R. Shanks, Phys. Rev. B 26 (1982) 1702.
[9] G. Hollinger, F.J. Himpsel, N. Martensson, B. Reihl, J. Doumerc and T. Akahane, Phys. Rev. B 27 (1983) 6370.
[10] R.G. Egdell, H. Innes and M.D. Hill, Surf. Sci. 149 (1985) 33.
[11] A. Magnéli, Acta Chem. Scand. 7 (1953) 315.
[12] P.Ph. Labbé, M. Goreaud, B. Raveau and J.C. Monier, Acta Crystallogr. B 34 (1978) 1433.
[13] M.L. Norton and L.G. Wolfe, Solid State Ionics 22 (1986) 75.
[14] B. Parkinson, J. Am. Chem. Soc. 112 (1990) 7498.
[15] J.B. Goodenough, in: Progress in Solid State Chemistry, Vol. 5, Ed. H. Reiss (Pergamon, New Jersey, 1971) p. 145.
[16] D.W. Bullett, J. Phys. C (Solid State Phys.) 16 (1983) 2197.
[17] J. Oi, A. Kishimoto and T. Kudo, J. Solid State Chem. 96 (1992) 13.